Polymorphism and solid state peculiarities in imidazo[1,5-a]pyridine core deriving compounds: An analysis of energetic and structural driving forces

Polymorphism and solid state peculiarities in imidazo[1,5-*a*]pyridine core deriving compounds: an analysis of the main energetic and structural differences.

Authors

Emanuele Priola[a]*, Eleonora Conterosito[b], Alessia Giordana[a], Giorgio Volpi[a], Claudio Garino[a], Luca Andreo[a], Eliano Diana[a], Claudia Barolo[a] and Marco Milanesio[b]

[a]Department of Chemistry, University of Turin, Via Pietro Giuria 9, Torino, Piemonte, 10125, Italy

[b]Dipartimento di Scienze e tecnologie Avanzate, Università del Piemonte Orientale, Via T. Michel 11, Alessandria, Italy, I-15121, Italy

Correspondence email: emanuele.priola@unito.it

Abstract The polymorphism and solid-state peculiarities of imidazo[1,5-*a*]pyridine derivatives have been investigated by a theoretical and experimental approach to shed light on the structural and energetic features of this family. Four couples of polymorphs and an ionic crystal form have been reported and analysed. Hirshfeld Surface and Energy Frameworks have been used to better understand the crystal packing features, in comparison with literature structures. The collection of all these characterizations made possible to analyse the differences between the polymorphs, the main energetic component dominating the crystal packing, and the effect of the different substitution on the central molecular skeleton on packing disposition. The assignment of vibrational spectra for the imidazo[1,5-*a*]pyridine core has been performed for the first time. Although the discussed polymorphs are very different in their crystal packing, from the energetic point of view they present a strong similarity. In all cases, the main interactions are π···π stacking and C-H···π to the aromatic rings, with some tendency to the formation of C-H···N contacts to the central imidazo[1,5a]pyridine nitrogen. The main energetic component is the dispersive one, with some contribution from the electrostatic component, and this situation is not modified by the presence of differing substituents. When hydrogen bond are present, the crystal packing is strongly modified and, energetically, the electrostatic component can overcome the dispersive on.

Keywords: Polymorphism, imidazo[1,5-*a*]pyridine, luminescence, vibrational spectroscopy, crystal packing, Energy Framework calculations, molecular interactions

1. Introduction

Polymorphism is one of the main research themes in the field of organic solid-state. The influence of this phenomenon in solid-state applications has been fully recognized in recent years: while the importance in pharmaceutics has been recognized since the historical cases of polymorphism-inducing impurities and problems, [1, 2] its influence in other important fields of materials science is now becoming increasingly studied and considered. The packing behavior may influence the resulting properties of luminescent materials, materials for solar cells (ex. inorganic-organic halide hybrid perovskites)[3] and high energy materials (propellants, explosives and pyrotechnics).[4-6] Polymorphism is the possibility of a molecule or of materials to crystallize with different crystal structures (having the same nature when melted) and, consequently, to show differences of their solid-state properties, influenced by symmetry and interactions.[7-13]

However, also in the case of applications that involve the dissolved molecule, this aspect must be considered, especially in the case of different solubilities or bio-availabilities for each crystal form or the formation of different clusters in solutions that can influence properties like luminescence.[14-16] An example are imidazo[1,5-*a*]pyridines derivatives.[17] These compounds have been employed in several pharmaceutical applications as HIV-protease inhibitors, cardiotonic agents, aromatase inhibitors in oestrogen-dependent diseases and thromboxane A2 synthetase inhibitors.[18-27] As UV-Vis absorbers, they have been used in a large variety of fields, including organic thin-layer field effect transistors and organic light emitting diodes.[28-31] Moreover, their application as ligands with different metals has been used to modulate optoelectronic properties.[32-39] In our research of new synthetic procedures to obtain derivatives of imidazo[1,5-*a*]pyridine, we noticed that a systematic solid-state study has not yet been carried out, despite relevant aspects of their crystallochemistry and an increasing number of crystal structure reported in CSD database (296 entries in CSD-version 5.41 update 3).[40-44] We decided to focalize our attention on neutral or cationic organic crystal structures, leaving the study of metal complexes to another paper. Thus, we selected five systems (Scheme 1), with both a single and a double imidazo[1,5-*a*]pyridine nucleus: 1-(pyridin-2-yl)-3-(4-(trifluoromethyl)phenyl)imidazo[1,5-*a*]pyridine (**1**), 3-(4-(*tert*-butyl)phenyl)-1-(pyridin-2-yl)imidazo[1,5-*a*]pyridine (**2**), 1,4-bis(1-(pyridin-2-yl)imidazo[1,5-*a*]pyridin-3-yl)benzene (**3**), 1,2-bis(1-(pyridin-2-yl)imidazo[1,5-*a*]pyridin-3-yl)ethane (**4**). These compounds have been crystallized in different solvents and several crystal forms have been detected and structurally characterized. At the same time, the effect of salification has been studied obtaining the nitrate salt for 2-(1-phenylimidazo[1,5-a]pyridin-3-yl)phenol (**5**). Crystal packing interactions have been investigated by means of Hirshfeld Surface and Energy Framework approaches, with the aim to analyze the energetic and interaction differences between the polymorphs of each selected molecule with a more accurate and comprehensive methodology.[45-50] Finally, the vibrational characterization, supported by DFT modelling, has been performed. The aim is to clearly state general trends observable in the crystal packing of imidazo[1,5-*a*]pyridines of interest for the research in this field.

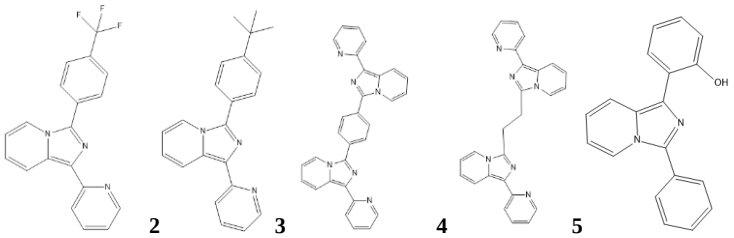

1 **2** **3** **4** **5**

Scheme 1 Molecular structures of **1**, **2**, **3**, **4** and **5**.

2. Experimental

2.1. Synthesis

All compounds were synthetized following the literature procedures.[21, 23, 36, 51-54] A list of the solvents employed for crystallization and the conditions of synthesis of each polymorph can be found in Table 1.

Crystal phase reported		Crystallization condition
Compound **1**	α form **1a**	Slow evaporation at room temperature of acetonitrile
	β form **1b**	Slow evaporation at room temperature of N,N'-dimethylformamide
Compound **2**	α form **2a**	Slow evaporation at room temperature of N,N'-dimethylformamide
	β form **2b**	Slow evaporation at room temperature of chloroform in presence of I_2
Compound **3**	α form **3a**	Slow evaporation at room temperature of N,N'-dimethylformamide
	β form **3b**	Slow evaporation at room temperature of acetonitrile
Compound **4**	hydrate form **4h**	Slow evaporation at room temperature of methanol in presence of acetic acid
	anhydrous form **4**	Slow evaporation at room temperature of N,N'-dimethylformamide
Compound **5**	nitrate salt **5n**	Slow evaporation at room temperature of ethanol in presence of $Al(NO)_3$

Table 1 Crystallization conditions for compounds **1**-**5**.

2.2. SCXRD measurements and structure resolution

Single crystal data of compound **1**-**5** were collected on a Gemini R Ultra diffractometer (Agilent Technologies UK Ltd., Oxford, U.K.) (except **4**, that was measured on a Xcalibur Sapphire 3) using graphite-monochromatic Mo Kα radiation (λ = 0.71073 Å) (for **1b**, **2a**, **2b**, **3a**, **3b**, **4**) or Cu Kα radiation (λ = 1.5406 Å) (for **1a** and **5n**) with the ω-scan method. CrysAlisPro software was used for retrieving cell parameters, for performing data reduction and for absorption correction (with multi-scan technique). All structures were solved by direct methods using ShelXS-14[55] and refined with full-matrix

least-squares on F^2 using the SHELXL-14[56] using Olex^2 program.[57] All non-hydrogen atoms were anisotropically refined. Hydrogen atoms were calculated and riding on the corresponding atom.

Structures images were obtained using Mercury software.[58] Crystal data and refinement, selected bonds lengths and angles amplitudes and asymmetric units of compounds are reported in ESI. The crystallographic data for **1**-**5** are deposited in Cambridge Crystallographic Data Centre as supplementary publications under the CCDC numbers 2081931-2081937 and 2045403. This information can be obtained free of charge from the Cambridge Crystallographic Data Centre via www.ccdc.cam.ac.uk/data_request/cifcodeCCDC.

2.3. Hirshfeld Surface and Energy Framework analysis

Crystal structures of **1**-**5** were processed to generate Hirshfeld Surfaces, fingerprint plots and Energy Frameworks with the program Crystal Explorer.[46] All Hirshfeld Surfaces were calculated in the highest resolution allowed by the program, and pairwise interaction for the calculation of Energy Frameworks was calculated with the B3LYP DFT method with the 6-31G(d,p) basis set, as implemented in Crystal Explorer.[46]

2.4. Raman and IR spectroscopic characterization

Spectra were recorded on crystalline or powder samples. FT-Raman spectra were obtained with a Bruker Vertex 70 spectrometer, equipped with the RAMII accessory, by exciting with a 1064 nm laser, with a resolution of 4 cm^{-1}. ATR-FTIR spectra were obtained in the range 4000-370 cm^{-1} with a Bruker Vertex 70 spectrophotometer equipped with the Harrick MVP2 ATR cell using DTGS detector, with a resolution of 4 cm^{-1}.

Computations were performed with the Gaussian 16 code, by employing the B3LYP hybrid density functional method with the 6-311G(d,p) basis set. Molecular geometry was optimized to an energy minimum and harmonic vibrational frequencies (Raman and IR) were computed.

3. Structural characterization

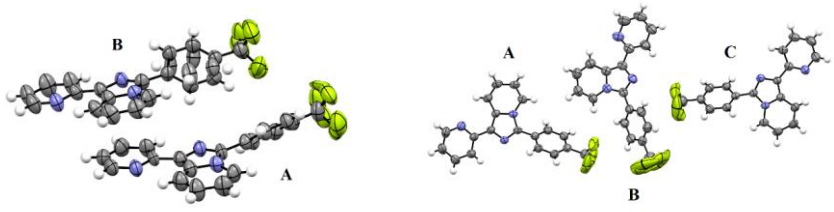

a) b)

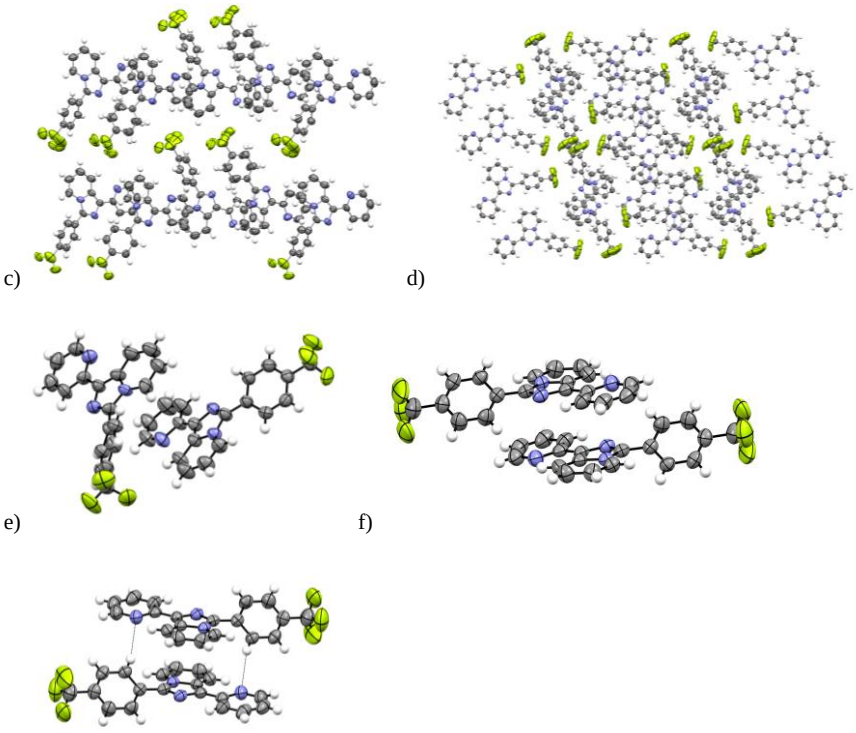

Figure 1 Asymmetric unit of form α (a) and form β (b) of **1**, and packing diagram of form α (c) and form β (d). π···π stacking details in form α (e) and in form β (f and g).

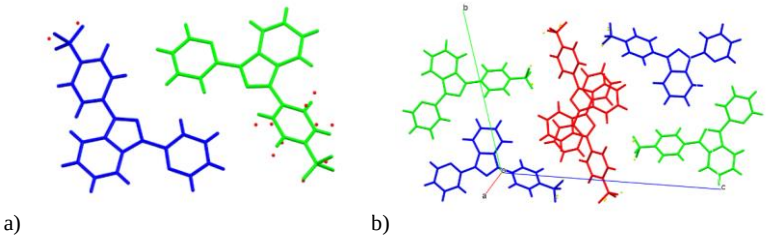

Figure 2 Pseudosymmetry relation between the two molecules in form α (a) and in form β (b) of compound **1**.

Two polymorphs have been found for compound **1**, form α (**1a**) from slow evaporation of N,N'-dimethylformamide and form β (**2b**) from slow evaporation of acetonitrile. The more relevant difference between them is the Z' multiplicity: in form α, two non-equivalent molecules can be found (see Figure 1a), while in form β three non-equivalent molecules can be observed (see Figure 1b). In the form α, the

two molecules differ for a two-position disorder affecting the phenyl ring substituted in position 3 of the imidazo[1,5*a*]pyridine core, that is rotated around the molecular axis (passing C12, C13, C16 and C17) of 29.01(10)° in one of the two molecules. Conversely, in form β, the three molecules have very similar conformations. As recently suggested by Clegg, Brock and Baggio,[59-62] the pseudosymmetry between non-crystallografically equivalent molecules was checked. In the case of form α (crystallized in $P2_1/c$ space group) by observing the two coplanar molecules in Figure 3a it is possible to notice that, although they are not generated from each other by a space group operation, most of the atoms are related by a local 2-fold axis perpendicular to the plane where the two molecule lies (or by an inversion center in the plane in the case of the smaller disorder component). On the other hand, in form β (crystallized in P-1 space group) it is possible to evidence (Figure 2b) the presence of local glide planes between green and blue non-equivalent molecules, while the red ones do not seem to be generated by local symmetry operations.

However, the two phases of **1** show quite different packing motifs, although the conformations of the molecules seem to be remarkably similar. The density of the two polymorphs is similar (1.420 g/cm^3 for α respect to 1.427 g/cm^3 for β), suggesting that the supramolecular architectures are similarly compact. Observing the disposition of the molecules in the α form (see Figure 1c), it is possible to observe layers of π···π stacked molecules in which the direction of the CF_3 groups is inverted every two molecules. In this layer, the imidazo[1,5*a*]pyridine core is stacked on the pyridine ring of the nearest molecule (inter-planar distance = 3.36(1) Å, see Figure 1e). Between the layers, the cited pseudosymmetry relation can be observed, inverting the disposition of the molecules. In the case of the β form, there are two stacking directions (see Figure 1d); at the borders of the unit cell, two series of molecules are ordered along the [010] axis in opposite directions, while in the middle of the unit cell the molecules are ordered along the [001] axis. Along the [100] direction, each layer interacts through π···π contacts with an inverted layer with the overlap of the imidazo[1,5*a*]pyridine core with the pyridyl substituent and vice versa in the case of green and blue molecules in Figure 2b (inter-planar distance = 3.63(1) Å, see Figure 1f). Red molecules in Figure 2d show π···π contacts between inverted imidazo[1,5*a*]pyridine cores supported by weak C-H···N (see Figure 1g and Figure 2b, interplanar distance of 3.521(9) Å between the imidazo[1,5*a*]pyridine cores, very low displacement).

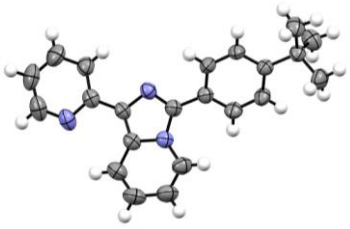

a)

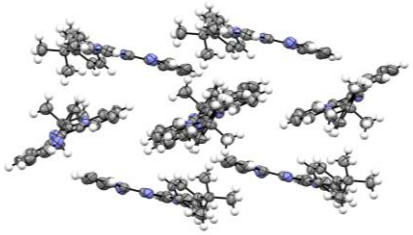

b)

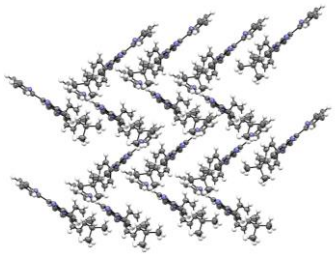

c)

Figure 3 Asymmetric unit of α form of **2** (a), packing rappresentation of α form along [101] direction (b) along and of β form along [100] (c).

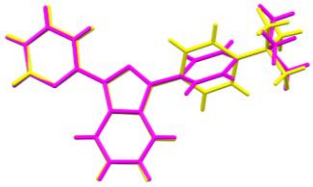

Figure 4 Overlap between the conformations of **2** in its α form (yellow) and its β form (pink).

Also compound **2** cristallyzes in two monoclinic structures, a centrosimmetric α phase in $P2_1/c$ from N,N'-dimetylformamide, and a non-centrosimmetric β phase in Cc from chlorophorm, but in presence of molecular iodide. The iodine was added with the aim of obtaining a halogen bonded-cocrystal, but no evidence of formation of a new cocrystal were observed. The two polimorphs are clearly distinguishable for their different morphology: the α form grows as long platelets, while the β form crystallizes in a bulky prismatic morphology, although the colour of the crystals is similar. Both crystal structures follow an herringbone pattern, but different aspects of the β form are worth noting: at first, the uncommon occurrence of a non-centrosymmetric space group in a crystal structure formed by a molecule without any chiral center.[63] This phenomenon can be due to the non planarity of the molecule in β form respect to α form (see Figure 4, interplanar angle N1-C12-C13-C14 of 54.89(10)° in β form, 34.42(8)° in α form) and to the packing arrangement (see Figure 3c), as already observed.[44] The herringbone disposition of the imidazo[1,5*a*]pyridine cores, specular to the rotated disposition followed by the 3-substituted phenyl groups, can induce polarity in the crystal structure of the β form, while the absence in α phase of this rotation creates a common centrosymmetric herringbone, similar to that of archetipal polyaromatics (see Figure 3b).[64-66] Another aspect to consider is the crystallization process: this phase could be obtained only in presence of molecular iodine, although no iodine has been found in the crystals. The interaction-induced nucleation of new phases is a known phenomenon, and some example of halogen bond-driven crystal growth have been reported.[67, 68]

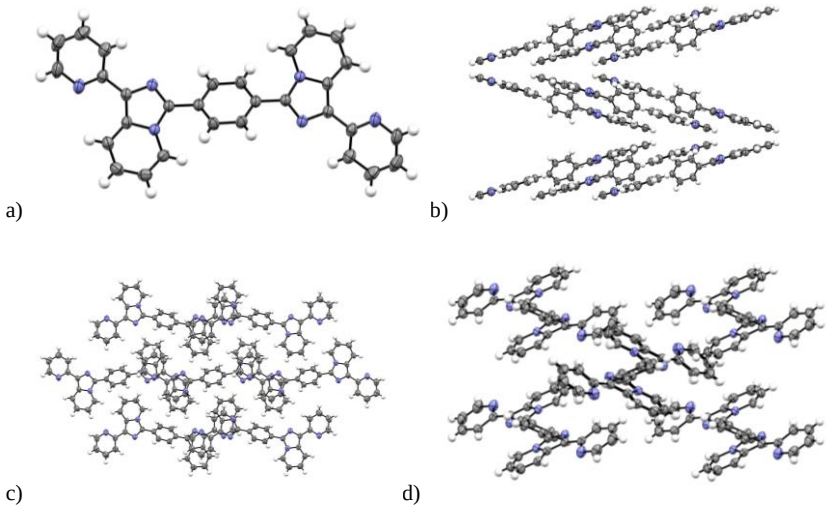

Figure 5 Asymmetric unit of α form of **3** (a), packing rappresentation of α form along [001] direction (b), a layer of the same structure **(c)** and of β form along [100] (d).

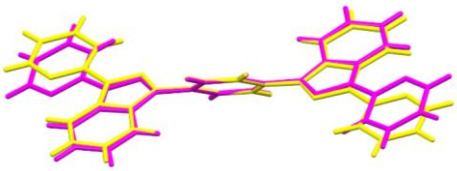

Figure 6 Overlap between the conformations of **3** in its α form (yellow) and its β form (pink).

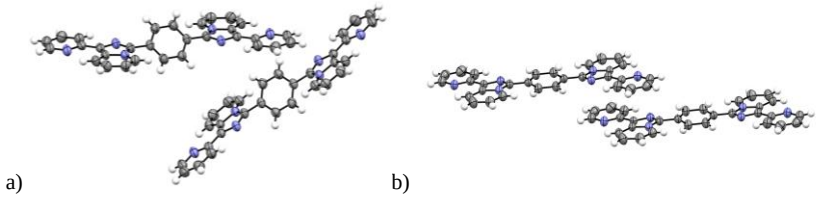

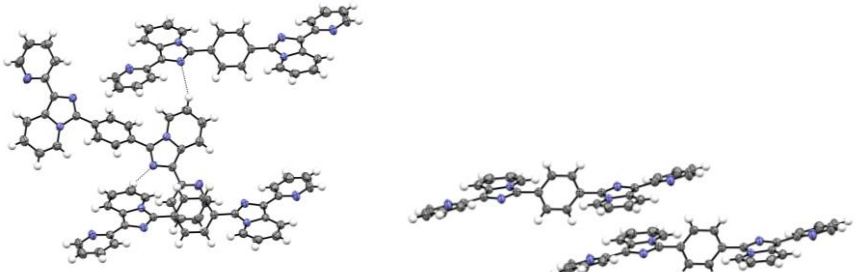

c) d)

Figure 7 Fragments of the crystal structure of **3a** (a and b) and of **3b** (c and d).

Compound **3** (Figure 5a) has a doubled imidazo[1,5*a*]pyridine core and two crystal forms have been identified: an orthorhombic α form, crystallized from DMF solvent and a monoclinic β form crystallized from acetonitrile. The molecular conformations in both crystal structures are very similar (Figure 6), with a torsion angle between the central phenyl ring in position 3 and the imidazo[1,5*a*]pyridine core of 43.97(10)° in α form and 46.35(8)° in β form. A larger difference is observed in the crystal packing disposition: in the α form the planar molecules are arranged in layers (see Figure 5c) interacting to each other only through dispersive forces and C-H···π contacts between the pyridine hydrogen and the imidazo[1,5*a*]piridine core (see Figure 7a). These layers are constructed by aromatic interactions between the planar fragments: as shown in Figure 7b, a pyridine group lies on the top of a imidazo[1,5*a*]piridine fragment for each couple of molecules. The monoclinic β form is more similar to a classical herringbone: the imidazo[1,5*a*]piridine cores are parallel along [001] interacting by π···π aromatic interactions (see Figure 7d). In the [010] direction the typical wavy structure is present, that is propagated by weak C-H···N contacts (see Figure 7c)

Compound **4** (Figure 8) crystallized in anhydrous form (**4**) and in the hydrated form (**4h**), reported in a previous pubblication,[43] both of them in a monoclinic space group. This is the only case in which two different conformations are present, although it is not possible to call them conformational polymorphs for the water presence.[11,69] Single crystals of **4h** and **4** were grown by slow evaporation of methanol in presence of acetic acid and slow evaporation of N,N'-dimethylformamide respectively at room temperature. These forms share the same lamellar habit and space group, but the packing shows remarkable differences and polymorph **4** is disordered. The main difference is observed in the single bond connecting the two planar moieties.

In fact, **4h** is planar with the central C-C single bond in the plane of the aromatic part while in **4** the C12 C13 atoms, bridging the two aromatic fragments of the molecule, are disordered and staggered, resulting in a torsional angle N3-C12a-C13a'-C13a'' of about 77°. The two halves of each molecule, therefore, lie on two different parallel planes, with a step of about 1Å. This part of the molecule is

disordered between the two possible up and down conformations due to the mobility of the singol C-C bond, with non equivalent occupancies (0.72 and 0.28, respectively, see Table S36).

The packing of **4h** viewed along a shows a γ-motif (Figure 8b) characterized by π···π stacking of the compound molecules and hydrogen bonds between a water molecule and the N2 atoms of two moieties. The packing of **4** is quite different and when viewed along c shows a sandwich herringbone motif (Figure 8d) with π···π stacking occurring along the ***a*** direction.[70, 71] These features suggest the ability of the molecule to behave differently in hydrous and anhydrous environment.

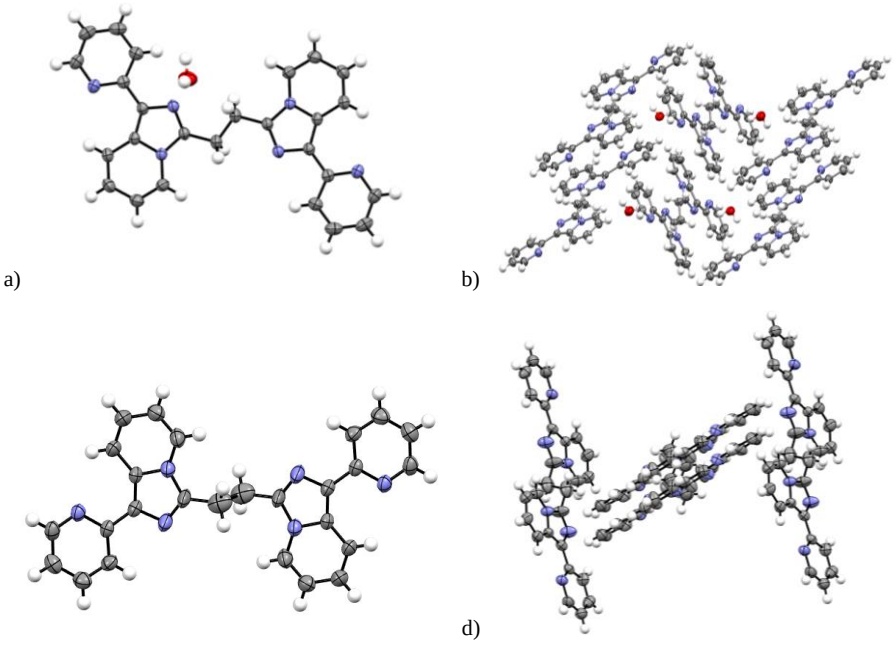

Figure 8 Asymmetric unit (a) and crystal packing (b) of **4h** from the literature[43] compared to those of **4** (c) and (d).

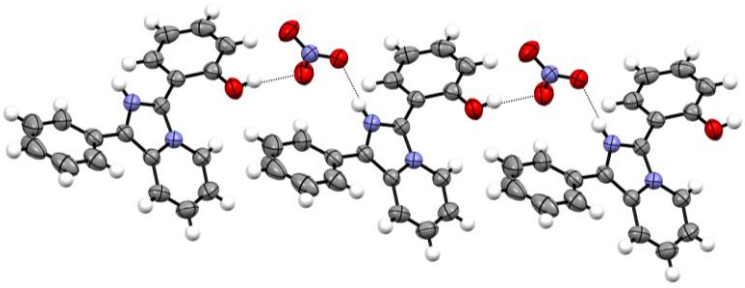

Figure 9 Hydrogen bond chain in the nitrate salt **5n**.

Interatomic distance	Neutral (Å)	Protonated (Å)
N1-C7	1.319(5)	1.336(3)
N1-C13	1.382(5)	1.369(3)
N2-C7	1.370(5)	1.355(3)
N2-C12	1.403(5)	1.404(3)
N2-C8	1.375(5)	1.388(3)
C12-C13	1.377(6)	1.380(3)
C12-C11	1.412(5)	1.420(3)
C11-C10	1.343(6)	1.341(5)
C10-C9	1.419(7)	1.421(5)
C9-C8	1.333(5)	1.340(5)

Table 2 Comparison of geometrical parameters in neutral (CCDC CODE: LOMCUM) and protonated (**5n**) imidazo[1,5*a*]pyridine core.

Finally, a protonated form of **5** was crystallized through hydrolysis of aluminium(III) nitrate, avoiding the use of HNO_3 for its oxidizing power. The crystal structure is deeply modified respect to the neutral form (CCDC CODE: LOMCUN)[33]: although the hydroxyl group acted as hydrogen bond donor to the nitrogen central site also in the neutral form, the presence of the acidic N-H donor and a good HB acceptor as NO_3^- makes possible the formation of a strongly bonded hydrogen bond chain (see Figure 9). The protonation, however, influences the conformation of the lateral group by a rotation around the Ph-imidazo[1,5*a*]pyridine connection different by that of neutral complex, probably to optimize the hydrogen bond geometry, while the molecular geometric parameters are not deeply influenced by the delocalized positive charge (see Table 2). This is confirmed by the geometrical parameters found in the alchilated imidazo[1,5-*a*]pyridine found in CSD (71 compounds).

After a careful analysis of the structural features of compounds **1**-**5**, all the polymorphs, although often similar in their molecular conformations, present very different crystal packings, in which the common motif is the inverted overlap of imidazo[1,5*a*]pyridine cores, when possible. This difference can be underlined with the program CrystalCMP, that compares the overall crystal packing of every structure without any cell or symmetry restriction.[72] By comparing all the couples (unless **4** and **4h**, showing different compositions), a very low degree of similarity is found in the crystal packing ($PS_{ab} > 15$ for all the couples). This is clearly observable also graphically by overlapping the clusters of the polymorphic crystal phases in Figure 10.

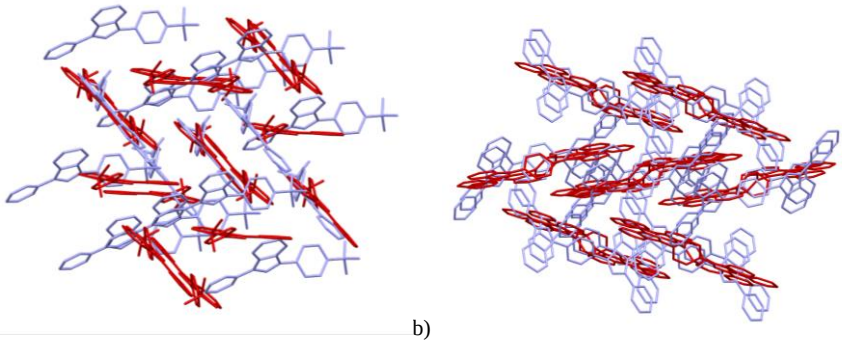

a) b)

Figure 10 Comparison by overlapping between crystal packing of **2a** (red) and **2b** (grey) (a) and between crystal packing of **3a** (red) and **3b** (grey) (b).

Moreover, it is important to notice that solvation (as in the case of **4**) or protonation of the central nitrogen (as in the case of **5**) can drastically modify both the crystal packing, and the main interactions and also the molecular conformation.

4. Hirshfeld Surface and Energy Framework analysis

Estimating the stability of different polymorphs through quantum-mechanical calculations is very difficult, because the difference in energy is very small, usually in the order of 1-4 kJ/mol, and anharmonicity and entropic components are an important part of this difference.[73, 74] However, the combination of the Hirshfeld Surface (H.S.) approach and the Pairwise calculation in the Energy Framework (E.F.) analysis can be used to underline (at least qualitatively) some energy and interaction differences or similarities between polymorphs.[50]

Hirshfeld Surface analysis allows to analyze the crystal structure of a molecule in a much more detailed level respect to the usual interatomic distance interpretation of the crystal packing: this instrument makes possible, although in an approximate manner, to describe the overall environment of a molecule, by considering the contacts all around its molecular volume.[49, 75]

At the same time, the Energy Framework approach, based on Pairwise energy calculations between nearby molecules, makes possible the decomposition of the energies of the interactions in 4 different components: E_{ele} (coulombic attraction), E_{pol} (polarization of molecules), E_{dis} (dispersive forces) and E_{rep} (repulsive energy, essential to the overall energy balance). In a parametric manner, but with very high accuracy, it is possible to analyze and describe the energetic components at the basis of a specific structure and compare them with other similar ones.[46]

We will first discuss the case of unsubstituted pyridyl imidazo[1,5-*a*]pyridine core, followed by the cases of 3-phenyl substituted pyridylimidazo[1,5-*a*]pyridines bearing different substituents (R = *t*-But, $-CF_3$, $-CH_3$, -OH, $-OCH_3$). These crystal structures have been chosen in literature and among the phases of **1** and **2** for the difference in steric hindrance and in electronegativity of the substituents. The effect of the presence of a heavy halogen and halogen bond on packing and energetic properties is also analyzed. At the same time, an energetic comparison between **5n** and its unprotonated correspondent (**5**) will be presented to understand the changes in energetic components of the protonation. Finally, the same analysis on doubled pyridyl imidazo[1,5-*a*]pyridine molecules, by comparing the crystal phases of **3** and **4** with molecules with a different degree of freedom and connection between the two imidazo[1,5-*a*]pyridine cores.

To start our analysis, the results of the unsubstituted molecular 3-(2-pyridinyl)imidazo[1,5-*a*]pyridine core were checked (CCDC Code: PRIMPY).[76] The structure of this compound can be described as a distorted herringbone caused by the asymmetric shape and shows undulated layers (see Figure S71). The π···π stacking and the C-H···π contacts are strong and pervasive all around the molecule: the first ones are involved in the typical disposition of the pyridyl group surrounding the imidazo[1,5*a*]pyridine core (and vice versa, 6.9 % of the Hirshfeld Surface, see Figure S73b and Table S78), while the second one is all around the aromatic system (9.6 %, see Figure S73c and Table S78). A strong C-H···N contact is also present toward the imidazo[1,5*a*]pyridine central nitrogen in position 2 (see Figure S73d and Table S78). From an energetic point of view, the main driving force is dispersive (see Figure S75-S77), with an intense interaction energy toward the neighboring stacking molecules (-35 kJ/mol) and weaker but more electrostatic interactions with the lateral ones in the plane (-11.9 kJ/mol with -6.2 kJ/mol of electrostatic component) (see Table S79).

Analyzing the couple of polymorphs of compound **1** ($-CF_3$ substitution on 3-phenyl ring), the different role of each non-equivalent molecule in the crystal packing is evidenced by a different percentage of interaction components on the H.S.: in the α form the molecule A has a lower percentage of π···π stacking (5.4 %) respect to molecule B (7.4%), but for both of them this contact is present on the pyridyl substituent on a face and on the imidazo[1,5*a*]pyridine core on the other face (see Figure S10b, Figure S12b and Table S43 and S45 for the numerical contribution of each contact). On the other hand, the percentage of C-H···π and C-H···F contacts are similar, with the first one dispersed on the pyridyl in position 1 and phenyl substituents in position 3 and the second one dominated by the presence of the

C-H of the central core (see Figure S10c, Figure S12c and Table S43 and S45). The situation of the three molecules in the β form is slightly different: while the π···π, C-H···F and the C-H···N contacts have similar percentage on the HS, although a different disposition around the shape of the molecule (es π···π is present only on the imidazo[1,5*a*]pyridine core, see Figure S17b, S18b and S21b, and see Table S48, S50 and S52 for the percentage), C-H···π contacts are different in the three cases for the different role of each asymmetric molecule in the crystal packing (see Figure S17c, S19c and S21c). By considering the pairwise interaction analysis and the Energy Frameworks, for both the crystal forms the main energetic component is dispersive, with the strongest interactions into couple of stacked molecules (40 kJ/mol approximately), suggesting a main role of Van der Waals interactions respect hydrogen bonds with a larger electrostatic component (see Figure S13-S15 and Figure S22-S24 for the E.F. representation and Table S46 and S53 for numerical values).[77, 78]

In the two polymorphs of compound **2** (*t*-But substituent on the 3-phenyl ring) the π···π interaction percentage is quite low (1.6 % for the α form and 0.8 % for the β form, see Table S55-S58), while the C-H···π contact has a more important role and is widespread overall the molecular volume (see Figure S26c and S31c). C-H···N interaction, as in the previous case, is directed to both the free N sites from phenyl C-H bonds for the β form and from the pyridinic ones in the α form (see Figure S26d and S31d). Considering the Pairwise interaction energies and the E.F., both the phases are dominated by dispersive forces with strong interactions among inclined stacked molecules in the α form (-41.9 kJ/mol and -32.5 kJ/mol, mainly dispersive, but with a good degree of electrostatic interaction for C-H···π interactions, see Table S56) and with the C-H···π interacting molecules in the β form (-42.2 kJ/mol and -31.0 kJ/mol, the first with a higher electrostatic component but also a strong repulsive one, the second mainly dispersive, see Table S59). However, although the different packing motifs, the main interaction energies are similar at this level of calculation as can be expected from the experimental results. The results obtained for this molecule can be compared to the results of LOMCOH molecule, in which a methyl meta substitution is present (see Figure S77).[33] This structure is peculiar for the non-centrosymmetric space group, probably caused by the hindered rotation of the phenyl group. As in the case of the polymorphs of **2**, the π···π and C-H···π interactions are the main driving force (4.1 % and 12.7 % of the H.S., see Figure S79b-c and Table S81), and to the neighbor molecules involved in these interactions mainly dispersive components are present (Figure S80-82 and Table S82).

By considering the analisys of the last reported compound **5n**, it is interesting to compare the results of H.S. and E.F. to the ones obtained from the unsalified molecule (CCDC code: LOMCUN).[33] In both cases, the main directional interaction is the hydrogen bond, in the case of unprotonated molecule from thr -OH fenolic group to the central imidazo[1,5*a*]pyridinic nitrogen atom in position 2, while in the protonated one from N-H and O-H groups to the nitrate anion, forming in both cases a ribbon of interacting molecules (see Figure 10 and Figure S83). Considering these structural features, it is not surprizing to find the signal of strong N-H···O interactions on the Hirshfeld Surface and on the

fingherprints (Figure 11a-d), and, in the perpendicular direction, the sign of π···π contacts (tipycal triangular motifs in the shape index reppresentation on H.S., see Figure 11 c-e), connecting the chains. Also in this case, a strong C-H··· π component is present (11% of the H.S., see Table S72). By considering the E.F. (Figure 12) and the pairwise interaction energies, it is clear the difference with the previous cases: the electrostatic component is comparable to the dispersive one, with energies of interaction to the nitrate anion of -58 kJ/mol, similar to the dispersive energy to π···π stacked molecules nearbye (see Table S73).

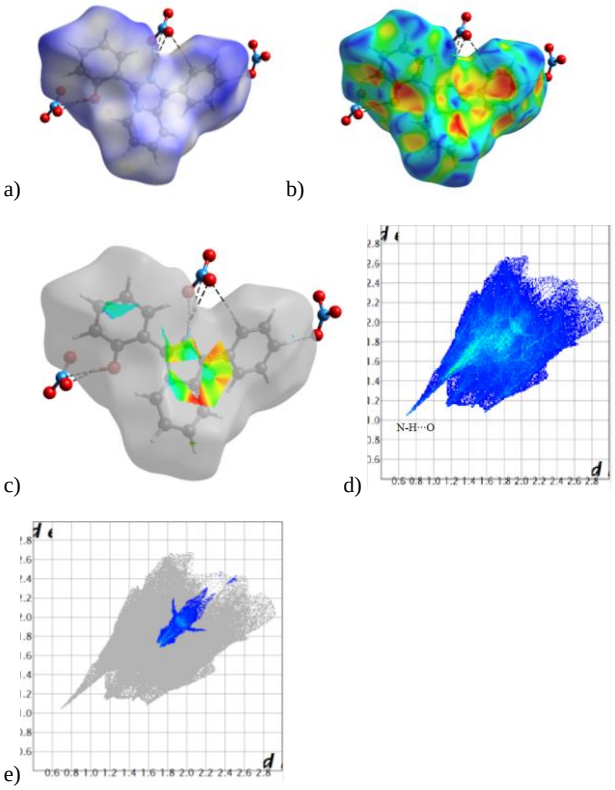

Figure 11 dnorm (a) and shape index (b) rappresentation on the Hirshfeld Surface of 5; general fingerprint plot (d) of **5**; π···π contact fraction (e) in the fingerprint plot and its localization on the Hirshfeld Surface (c).

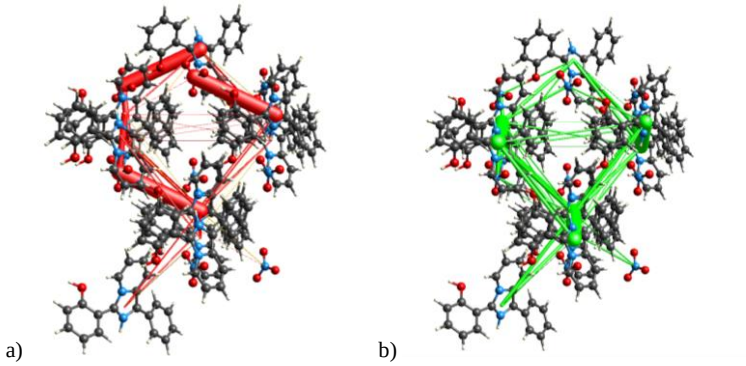

a) b)

Figure 12: Coulombic Energy Framework component (a) and dispersive Energy Framework component (b) for the protonated phase of **5**.

By looking at the neutral crystal structure, the π···π contacts are less pronounced (3.6% of the H.S., only on a face of the molecule, see Figure S85b and Table S84) and C-H··· π component are more evident (15.1% of the H.S., all arround the molecule, see Figure S85c and Table S84). However, the driving force of the crystallization is the O-H···N interaction, as suggested by the Pair interaction energies (see Table S85). In this case, the main interactions are toward the hydrogen bonded molecules, with interaction energy of -74.1 kJ/mol. It is worth noting that also in this case the predominat component of this energy is electrostatic (-86.1 kJ/mol) one (see Table S85), and all the other dispersive interaction energies are smaller.

To further understand the effect of substituents, other selected molecules from the literature were analysed. An example of electronegative substituent is the case of LOZJOZ,[79] showing a methoxy and a fenolic group, and the cases of halide substituents in NOXLUK and NORMAR were chosen.[42] In the first case, the crystal structure is dominated by the presence of O-H···N interactions able to impose a spiral pattern (although the meta position of the phenolic group should interfere in the formation of these interactions, see Figure S89). π···π and C-H··· π component are both high (5.3 % and 13.1 % of the H.S., respectively, see Figure S91b-c and Table S87), but a strong C-H···O component is present toward the methoxy substituent (5.7 % of the H.S., see Figure S91e and Table S87). Also in this case, the stronger interaction is directed toward the hydrogen bonded molecules (-64,4 kJ/mol, with a strong electrostatic component, -48.6 kJ/mol, but also a strong dispersive one, -56.2 kJ/mol, see Table S88), and weaker dispersive interactions are directed to the other nearby molecules (-49.7 kJ/mol and -27.0 kJ/mol, respectively, see Table S88).

For the bromide and iodide substituted molecules NOXLUK and NORMAR, the H.S. analysis has been already reported,[42] but some more in dept insight can be obtained with the Energy Framework analisys.

In both cases, the main interactions are dispersive and are directed to the π···π stacked molecules in the layer (see Figure S101-S105), with a very similar energy in the two cases (-40.5 kJ/mol, see Tables S92 and S93), demonstrating that at this level of calculation the two crystal environments are equivalent and the difference in the heavy halogen atom does not greatly influence the energetic of the crystals.

Analysing α and β forms of **3**, the first double imidazo[1,5*a*]pyridine core molecule examined, the difference in the interactions between the crystal forms seems larger with respect to the other cases: π···π interactions are dominant in the α form respect to the β form in which is almost absent (7.5 %, localized on one half for each face of the molecule, respect to 1.6 %, see Figure S36b and S41b, Table S61 and S66 for the numerical values). On the contrary, in the β phase a greater influence of C-H···π interaction on the H.S. can be observed, with a higher percentage and a diffuse presence overall the molecule, while in the case of the α form this interaction is evident only on the imidazo[1,5*a*]pyridine core from the C-H of pyridyl moiety (see Figure S36c and S41c, Table S61 and S66 for the numerical values). Also in this case, for both the polymorphs the dispersion is the dominant contribution. Two main interactions are present in the α form, one with π···π stacked molecules (E_{tot}= -43.3 kJ/mol, of which -74.1 kJ/mol of the dispersion component) and another with C-H···π interacting molecules (-37.9 kJ/mol, with a greater electrostatic component of -11.3 kJ/mol, see Table S62). In the case of β form, the main interaction is with the two laterally overlapped molecules and has a very high part of dispersion energy (-57.1 kJ/mol, of which -81 kJ/mol are from dispersion and -12.7 kJ/mol are from electrostatics), while the other one is with the four C-H···π interacting molecules and is slightly more electrostatic in nature (38.5 kJ/mol and E_{el}: -15.3 kJ/mol, see Table S66). As can be noticed, in the β form in which the C-H···π interactions are stronger than in the α form, the electrostatic component is stronger, although the dispersion forces are the main driving force in both cases.

To further investigate the driving forces guiding the crystal packing of the double pyridyl imidazo[1,5-*a*]pyridine molecules, the result obtained for **3** are compared with two compounds in which the two imidazo[1,5*a*]pyridine core are directly connected (CCDC Code: GEJZEB)[80] or the central meta phenyl substitution imposes a distortion from planarity (CCDC Code: SUZBIA)[44]. GEJZEB structure shows a classical herringbone motif, similar to the classical polyaromatic molecules for its complete planarity (see Figure S65), while the SUZBIA displays a helical disposition that is, however, a distortion of the same motif and results in a non-centrosymmetric pattern (see Figure S95). By looking at the H.S. analysis, the planar molecule shows an increase in π···π contacts (disposed asymmetrically on the two molecular surfaces on the pyridyl and on the imidazo[1,5*a*]pyridine core, respectively), although the C-H···π contacts remain the main directional contacts (see Table S75 and Figure S67b-c). The SUZBIA crystal packing, on the other hand, is dominated by C-H···π contacts (17.8% of the HS) and the π···π contacts are diminished (3 % of the H.S.) due to the steric constrains of the rotation (see Table S90 and Figure S97b-c). By looking at the E.F. analysis, GEJZEB shows strong dispersive components (the two typical strong interaction of herringbone of -75.1 KJ/mol along the column and interactions with -20.2

kJ/mol of energy with the nearest neighbors outside, but in both the cases very low electrostatic component, see Figure S68-S70 and Table S76), while in the crystal structure SUZBIA, although the dispersive component is also dominant, the pairwise interactions have a greater electrostatic component due to the dominant C-H···π contacts (see Figure S98-S100, Table S91). These results suggest that, although all these molecules with large aromatic surfaces tends to form the herringbone pattern, the introduction of a further degree of freedom with a central phenyl group can induce distortions in the pattern and can generate polymorphism or non-centrosymmetric space groups.

In the case of the hydrate form of compound **4**, **4h**, the Hirshfeld Surface analysis is already reported in the original publication,[43] while for the anhydrous form, **4**, is reported here for the first time. In this sense, it is interesting to compare the results of the H.S. generated for the two components of the disorder in the central part of the molecule in **4**. In the main component (for the frequency of the two components, see Table S36), the larger differences with respect to the minor one can be observed in the distribution and percentage of C-H···π and π···π contacts: in the first component the π···π contacts are more pronounced, although in the minor component they are shorter while for C-H···π contacts is the opposite, since they are more pronounced in the minor component with respect to the other one (see Table S67 and Table S69). In both cases, strong C-H···N contacts are directed to the central imidazo[1,5*a*]pyridine nitrogen from the alkane fragment (see Figure S51e and Figure S56e). By looking at the H.S. of **4h**, it is clear the strongest and shortest interaction is the hydrogen bond between water and the central nitrogen, although strong C-H···O contacts are also present in the channels formed by the solvent. Moreover, C-H···π and π···π contacts are also present and stabilize the organic framework surrounding the water channels. Considering the E.F. analysis, it is interesting to notice that in the hydrate form, **4h**, two different major interaction components can be observed: a strong dispersive attraction (-49.5 kJ/mol) between the stacked molecules and a strong electrostatic interaction with the water molecule due to the OH···N strong hydrogen bond (see Figure S45-S47 and Table S66). Comparing the results obtained for **4h** to those of the anhydrous **4**, all the main interaction components are dispersive in nature and are directed to nearby stacked molecules (see Table S68 and S60). At the same time, it is quite suggestive that the percentage of the two-component disorder in **4** is supported by a difference in the Pairwise interaction energies in the two cases. By looking at the strongest interaction calculated in the two divided components, in the most probable one the energy is -79.8 kJ/mol and is directed toward the two nearest packing neighbors, while in the less probable one the energy is -77.2 kJ/mol, directed toward the same couple of molecules (see Table S68 and Table S70). By looking in detail at the reasons of this energetic difference, at this level of calculation, the main feature is a higher repulsive energy in the case of less probable disorder component (see Table S68 and Table S70).

Hirschfeld Surface and Energy Framework analysis indicated that, without any strong hydrogen bond donor or acceptor, the main interactions are π···π and C-H···π, with a strong tendency to the formation of C-H···N weak interaction when the geometry is optimal. This conclusion is also well supported by

the interaction energies calculated, that are mainly dispersive or weakly electrostatic, and not strongly influenced by the different substituent analyzed. In general, however, the packing motifs can be reconducted to the herringbone motif or some distortion of it. The larger differences are present when helical pattern can be obtained for hindered groups or sterically demanding substituents.[71] When strong hydrogen bond donor and acceptors are present, strong hydrogen bonds between them are the driving force of the packing, and the electrostatic component becomes of the same strength of the dispersion component or dominant. However, often no strong energetic difference between also clearly structurally different polymorphs is present, as expected, but the structural differences are clear in the H.S. analysis of the interaction components.

5. Vibrational characterization

For the first time, the assignment of the vibrational modes of imidazo[1,5-*a*]pyridine derivatives has been done according to the computed frequencies calculated with a DFT method (see Table S71-72) and to experimental Raman and IR spectra (Figure S112-S117). In general, below 1650 cm^{-1} stretching (ν), bending (δ) and deformation (γ) modes of aromatic rings can be observed, while around 3000 cm^{-1} there are signals related to the stretching modes of C–H. At low wavenumber torsional (τ) modes can be observed. Some features were pointed out from the comparison between the spectra of compound **1**, **2** and **3** respect to the experimental and calculated spectra of unsubstituted 1-(2-pyridyl)-3-phenylimidazo[1,5-*a*]pyridine (**6**), employed in previous studies (see Scheme 2).[36, 39, 54]

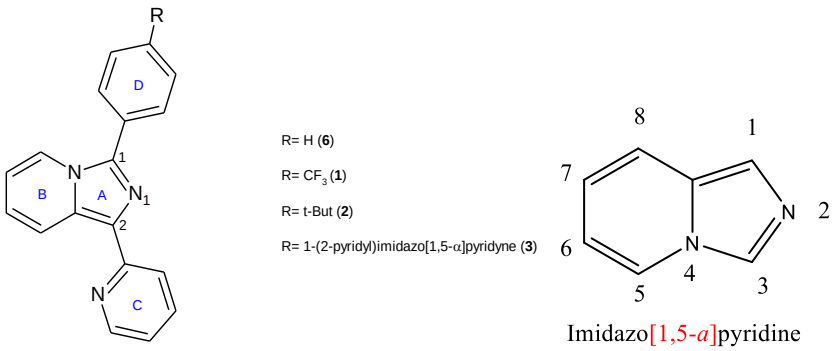

Scheme 2. Molecular structure and numbering of compound **6** and its derivatives.

At high wavenumbers, the pattern of these compounds is similar, except for the signals of stretching modes of aliphatic C–H groups below 3000 cm^{-1} that are present only in the spectra of compound **2** and **4**. In the spectral range 1650-1500 cm^{-1} there are the most intense Raman signals, related to stretching modes (ν) of aromatic rings. Calculations indicate that signals at 1631, 1603 and 1585 cm^{-1} are mainly attributable to stretching mode of a specific ring, respectively B, D and C. The substitution effect is evident for the signals assigned to ν (ring D) and for the signal mainly attributable to the stretching of

interring bond between A and D rings (at 1533 cm^{-1}), both shift by up to 20 cm^{-1} in the spectra of **1**, **2** and **3**. In the spectral range 1500-1000 cm^{-1}, stretching and bending (δ) modes of aromatic rings can be observed. In the IR spectrum of **3**, strong signals related to methyl group modes at 1482, 1470, 1459, 1400, 1390, 1365, 1357 cm^{-1}, can be observed, while for **4** only a signal at 1371 cm^{-1} can be attributed to the bending of the $–CH_2$ groups. In the IR spectrum of **1**, strong broad signal related to $–CF_3$ modes can be observed around 1320 cm^{-1} and between 1170-1060 cm^{-1}. For all compounds, signals of breathing modes of aromatic rings appear in the Raman spectra below 1150 cm^{-1}, in concomitance with out-of-plane deformation modes (γ). In particular, a sharp medium intense peak at 980 cm^{-1} (assigned to breathing mode) remains virtually unchanged in all compounds and could be used to confirm coordination in corresponding metal complexes. On the contrary, the IR spectra are more intricate due to the strong intensity of γ modes.

The spectra of the neutral form of compound **5** (powder form obtained from synthesis) were compared to thoseof **6**. The presence of phenyl or pyridyl ring leads to some difference in the IR-Raman spectra: the strong signal related to stretching mode of ring C shifts for effect of nitrogen substitution (1600 (**5**)/1587 (**6**) cm^{-1}), but similar shifts and different intensity are observed at low wavenumbers for signals attributable to modes of ring C and D. The Raman spectrum of the salt form (**5n**) is analogous to that of the neutral form **5**, instead in the IR spectrum the presence of hydrogen bonds is confirmed by the strong and broad signal above 3000 cm^{-1}. The NO_3 asymmetric stretching modes also leadto a broadening in range 1400-1300 cm^{-1}, ascribable to hydrogen bond chain formation ($NH^+\cdots NO_3^-\cdots OH$) and to an overlapping with δ(NH) mode.

6. Conclusions.

A set of 3 polymorphic structures, a pseudo-polymorphic one and a salified compound, based on imidazo[1,5-*a*]pyridine core, has been analyzed from a crystallographic, energetic and vibrational viewpoints. Although the discussed polymorphs are very different in their crystal packing, as can be seen from both visual inspection and Hirshfeld Surface analysis, from the energetic point of view they present a strong similarity. In all cases, the main interactions are π···π stacking between inverted molecules and C-H···π to the aromatic rings, with some tendency to the formation of C-H···N contacts to the central imidazo[1,5*a*]pyridine nitrogen. The main energetic component is the dispersive one, with some contribution from the electrostatic component, and this situation is not modified by the presence of differing substituents. In general, without any strong hydrogen bond donor or acceptor, the crystal packing can be seen as a modification of the classical herringbone motif, typical of polyaromatic compounds. Some clear exceptions are the couple of polymorphs of **1**, due to Z'>1 in both cases, and sterically hindered molecules like GEIZEB or **4h**, that form helical motifs. This theme is linked to a peculiar fact in the crystallochemistry of imidazo[1,5*a*]pyridine derived molecules: in this family, a very high frequency of non-centrosymmetric crystal structure is observed, although no chiral center has been added to them (see FigureS111). This is a rare and interesting aspect, that can be used for the

synthesis of new materials showing NLO properties or other functional properties linked to non-centrosymmetric solid-state disposition. Finally, when strong hydrogen bond donors and acceptors are present, the crystal packing is strongly modified by the presence of these directional interactions and, energetically, the electrostatic component can overcome the dispersive one. Moreover, protonation of the central nitrogen (as in **5p)** can deeply modify the crystal structure of the original molecule, by enhancing the electrostatic component and by changing the hydrogen bond network, although no strong modification in the molecular geometry has been observed.

References

1. J. Haleblian and W. McCrone, *Journal of Pharmaceutical Sciences*, 1969, **58**, 911-929.
2. A. D. Bond, R. Boese and G. R. Desiraju, *Angewandte Chemie International Edition*, 2007, **46**, 618-622.
3. O. J. Weber, D. Ghosh, S. Gaines, P. F. Henry, A. B. Walker, M. S. Islam and M. T. Weller, *Chemistry of Materials*, 2018, **30**, 3768-3778.
4. Z.-Q. Zhang, W. Qian, H. Lu, W. Yang, C. Zhang, G. Fan and Q. Ma, *Crystal Growth & Design*, 2020, **20**, 8005-8014.
5. F. P. A. Fabbiani and C. R. Pulham, *Chemical Society Reviews*, 2006, **35**, 932-942.
6. K. M. Anderson, M. R. Probert, C. N. Whiteley, A. M. Rowland, A. E. Goeta and J. W. Steed, *Crystal Growth & Design*, 2009, **9**, 1082-1087.
7. R. Purohit and P. Venugopalan, *Resonance*, 2009, **14**, 882.
8. D. Braga, F. Grepioni, L. Maini and M. Polito, in *Molecular Networks*, ed. M. W. Hosseini, Springer Berlin Heidelberg, Berlin, Heidelberg, 2009, DOI: 10.1007/978-3-642-01367-6_7, pp. 87-95.
9. A. J. Cruz-Cabeza, S. M. Reutzel-Edens and J. Bernstein, *Chemical Society Reviews*, 2015, **44**, 8619-8635.
10. S. Price, *Acta Crystallographica Section B*, 2013, **69**, 313-328.
11. A. J. Cruz-Cabeza and J. Bernstein, *Chemical Reviews*, 2014, **114**, 2170-2191.
12. A. Gavezzotti, *Journal of Pharmaceutical Sciences*, 2007, **96**, 2232-2241.
13. K. Kersten, R. Kaur and A. Matzger, *IUCrJ*, 2018, **5**, 124-129.
14. M. Pudipeddi and A. T. M. Serajuddin, *Journal of Pharmaceutical Sciences*, 2005, **94**, 929-939.
15. Y. Kobayashi, S. Ito, S. Itai and K. Yamamoto, *International Journal of Pharmaceutics*, 2000, **193**, 137-146.
16. B. Lu, S. Liu and D. Yan, *Chinese Chemical Letters*, 2019, **30**, 1908-1922.
17. G. Volpi and R. Rabezzana, *New Journal of Chemistry*, 2021, **45**, 5737-5743.
18. D. Davey, P. W. Erhardt, W. C. Lumma, J. Wiggins, M. Sullivan, D. Pang and E. Cantor, *Journal of Medicinal Chemistry*, 1987, **30**, 1337-1342.
19. B. P. Fauber, A. Gobbi, K. Robarge, A. Zhou, A. Barnard, J. Cao, Y. Deng, C. Eidenschenk, C. Everett, A. Ganguli, J. Hawkins, A. R. Johnson, H. La, M. Norman, G. Salmon, S. Summerhill, W. Ouyang, W. Tang and H. Wong, *Bioorganic & Medicinal Chemistry Letters*, 2015, **25**, 2907-2912.
20. S. Fuse, T. Ohuchi, Y. Asawa, S. Sato and H. Nakamura, *Bioorganic & Medicinal Chemistry Letters*, 2016, **26**, 5887-5890.
21. M. A. Ingersoll, A. S. Lyons, S. Muniyan, N. D'Cunha, T. Robinson, K. Hoelting, J. G. Dwyer, X. R. Bu, S. K. Batra and M.-F. Lin, *PLOS ONE*, 2015, **10**, e0131811.
22. D. Kim, L. Wang, J. J. Hale, C. L. Lynch, R. J. Budhu, M. MacCoss, S. G. Mills, L. Malkowitz, S. L. Gould, J. A. DeMartino, M. S. Springer, D. Hazuda, M. Miller, J. Kessler, R. C. Hrin, G. Carver, A. Carella, K. Henry, J. Lineberger, W. A. Schleif and E. A. Emini, *Bioorganic & Medicinal Chemistry Letters*, 2005, **15**, 2129-2134.
23. S. Priyanga, T. Khamrang, M. Velusamy, S. Karthi, B. Ashokkumar and R. Mayilmurugan, *Dalton Transactions*, 2019, **48**, 1489-1503.
24. M. Roy, B. V. S. K. Chakravarthi, C. Jayabaskaran, A. A. Karande and A. R. Chakravarty, *Dalton Transactions*, 2011, **40**, 4855-4864.
25. F. Yagishita, J.-i. Tanigawa, C. Nii, A. Tabata, H. Nagamune, H. Takanari, Y. Imada and Y. Kawamura, *ACS Medicinal Chemistry Letters*, 2019, **10**, 1110-1114.
26. A. Kamal, A. V. S. Rao, V. L. Nayak, N. V. S. Reddy, K. Swapna, G. Ramakrishna and M. Alvala, *Organic & Biomolecular Chemistry*, 2014, **12**, 9864-9880.
27. T.-c. Liu, X. Peng, Y.-c. Ma, Y.-c. Ji, D.-q. Chen, M.-y. Zheng, D.-m. Zhao, M.-s. Cheng, M.-y. Geng, J.-k. Shen, J. Ai and B. Xiong, *Acta Pharmacologica Sinica*, 2016, **37**, 698-707.
28. E. Fresta, G. Volpi, C. Garino, C. Barolo and R. D. Costa, *Polyhedron*, 2018, **140**, 129-137.
29. A. Irfan, A. R. Chaudhry, A. G. Al-Sehemi, M. A. Assiri and A. Hussain, *Computational Materials Science*, 2019, **170**, 109179.
30. D. R. Mohbiya and N. Sekar, *ChemistrySelect*, 2018, **3**, 1635-1644.
31. M. D. Weber, C. Garino, G. Volpi, E. Casamassa, M. Milanesio, C. Barolo and R. D. Costa, *Dalton Transactions*, 2016, **45**, 8984-8993.

ha formattato: Italiano (Italia)

ha formattato: Italiano (Italia)

ha formattato: Italiano (Italia)

32. G. A. Ardizzoia, S. Brenna, S. Durini and B. Therrien, *Polyhedron*, 2015, **90**, 214-220.
33. G. A. Ardizzoia, S. Brenna, S. Durini, B. Therrien and M. Veronelli, *European Journal of Inorganic Chemistry*, 2014, **2014**, 4310-4319.
34. G. A. Ardizzoia, G. Colombo, B. Therrien and S. Brenna, *European Journal of Inorganic Chemistry*, 2019, **2019**, 1825-1831.
35. G. A. Ardizzoia, D. Ghiotti, B. Therrien and S. Brenna, *Inorganica Chimica Acta*, 2018, **471**, 384-390.
36. A. M. Blanco-Rodríguez, H. Kvapilová, J. Sýkora, M. Towrie, C. Nervi, G. Volpi, S. Záliš and A. Vlček, *Journal of the American Chemical Society*, 2014, **136**, 5963-5973.
37. G. Volpi, E. Priola, C. Garino, A. Daolio, R. Rabezzana, P. Benzi, A. Giordana, E. Diana and R. Gobetto, *Inorganica Chimica Acta*, 2020, **509**, 119662.
38. E. Priola, G. Volpi, R. Rabezzana, E. Borfecchia, C. Garino, P. Benzi, A. Martini, L. Operti and E. Diana, *Inorganic Chemistry*, 2020, **59**, 203-213.
39. L. Salassa, C. Garino, A. Albertino, G. Volpi, C. Nervi, R. Gobetto and K. I. Hardcastle, *Organometallics*, 2008, **27**, 1427-1435.
40. G. Volpi, G. Magnano, I. Benesperi, D. Saccone, E. Priola, V. Gianotti, M. Milanesio, E. Conterosito, C. Barolo and G. Viscardi, *Dyes and Pigments*, 2017, **137**, 152-164.
41. G. Volpi, B. Lace, C. Garino, E. Priola, E. Artuso, P. Cerreia Vioglio, C. Barolo, A. Fin, A. Genre and C. Prandi, *Dyes and Pigments*, 2018, **157**, 298-304.
42. G. Volpi, C. Garino, E. Priola, C. Magistris, M. R. Chierotti and C. Barolo, *Dyes and Pigments*, 2019, **171**, 107713.
43. G. Volpi, C. Garino, E. Priola, E. Diana, R. Gobetto, R. Buscaino, G. Viscardi and C. Barolo, *Dyes and Pigments*, 2017, **143**, 284-290.
44. G. Volpi, C. Garino, E. Conterosito, C. Barolo, R. Gobetto and G. Viscardi, *Dyes and Pigments*, 2016, **128**, 96-100.
45. D. Dey, S. P. Thomas, M. A. Spackman and D. Chopra, *Chemical Communications*, 2016, **52**, 2141-2144.
46. C. F. S. Mackenzie, P.R.; Jayatilaka, D.; Spackman M.A., *IUCrJ*, 2017, **4**, 575--587.
47. S. L. J. Tan, M.M.; Tiekink, E.R.T. , *Acta Crystallographica Section E*, 2019, **75**, 308--318.
48. C. Wang and C. C. Sun, *Crystal Growth & Design*, 2018, **18**, 1909-1916.
49. J. J. McKinnon, D. Jayatilaka and M. A. Spackman, *Chemical Communications*, 2007, DOI: 10.1039/B704980C, 3814-3816.
50. J. J. McKinnon, F. P. A. Fabbiani and M. A. Spackman, *Crystal Growth & Design*, 2007, **7**, 755-769.
51. F. Yagishita, N. Kozai, C. Nii, Y. Tezuka, N. Uemura, Y. Yoshida, T. Mino, M. Sakamoto and Y. Kawamura, *ChemistrySelect*, 2017, **2**, 10694-10698.
52. F. Yagishita, T. Kinouchi, K. Hoshi, Y. Tezuka, Y. Jibu, T. Karatsu, N. Uemura, Y. Yoshida, T. Mino, M. Sakamoto and Y. Kawamura, *Tetrahedron*, 2018, **74**, 3728-3733.
53. C. Garino, T. Ruiu, L. Salassa, A. Albertino, G. Volpi, C. Nervi, R. Gobetto and K. I. Hardcastle, *European Journal of Inorganic Chemistry*, 2008, **2008**, 3587-3591.
54. G. Volpi, C. Garino, L. Salassa, J. Fiedler, K. I. Hardcastle, R. Gobetto and C. Nervi, *Chemistry – A European Journal*, 2009, **15**, 6415-6427.
55. G. M. Sheldrich, *Acta Crystallographica Section A*, 2008, **64**, 112--122.
56. G. M. Sheldrich, *Acta Crystallographica Section A*, 2015, **71**, 3--8.
57. L. J. B. O. V. Dolomanov, R. J. Gildea, J. A. K. Howard, H. Puschmann, *Journal of Applied Crystallography*, 2009, **42**, 339--341.
58. I. J. B. C. F. Macrae, J. A. Chisholm, P. R. Edgington, P. McCabe, E. Pidcock, L. Rodriguez-Monge, R. Taylor, J. van de Streek, P. A. Wood, *Journal of Applied Crystallography*, 2008, **41**, 466--470.
59. R. Baggio, *Acta Crystallographica Section C*, 2020, **76**, 258--268.
60. W. Clegg, *Acta Crystallographica Section E*, 2019, **75**, 1812--1819.
61. R. Baggio, *Acta Crystallographica Section C*, 2019, **75**, 837--850.
62. B. C.P., *Acta Crystallographica Section C*, 2019, **75**, 835--836.
63. E. Pidcock, *Chemical Communications*, 2005, DOI: 10.1039/B505236J, 3457-3459.
64. G. R. Desiraju, Gavezzotti, A., *Acta Crystallographica Section B*, 1989, **45**, 473--482.
65. A. Gavezzotti, Desiraju, G.R., *Acta Crystallographica Section B*, 1988, **44**, 427--434.
66. G. R. Desiraju and A. Gavezzotti, *Journal of the Chemical Society, Chemical Communications*, 1989, DOI: 10.1039/C39890000621, 621-623.
67. G. Cavallo, P. Metrangolo, R. Milani, T. Pilati, A. Priimagi, G. Resnati and G. Terraneo, *Chemical Reviews*, 2016, **116**, 2478-2601.
68. P. Metrangolo and G. Resnati, *Chemistry – A European Journal*, 2001, **7**, 2511-2519.
69. A. Nangia, *Accounts of Chemical Research*, 2008, **41**, 595-604.
70. V. Toson, M. Milanesio and E. Conterosito, *Zeitschrift für Kristallographie - Crystalline Materials*, 2017, **232**, 463-469.
71. L. Loots and L. J. Barbour, *CrystEngComm*, 2012, **14**, 300-304.
72. E. S. J. Rohlícek, M. Babor, J. Cejka, *Journal of Applied Crystallography*, 2016, **49**, 2172--2183.
73. J. Hoja, H.-Y. Ko, M. A. Neumann, R. Car, R. A. DiStasio and A. Tkatchenko, *Science Advances*, 2019, **5**, eaau3338.
74. A. Burger and R. Ramberger, *Microchimica Acta*, 1979, **72**, 259-271.
75. M. A. Spackman and D. Jayatilaka, *CrystEngComm*, 2009, **11**, 19-32.
76. F. Shibahara, A. Kitagawa, E. Yamaguchi and T. Murai, *Organic Letters*, 2006, **8**, 5621-5624.
77. G. R. Desiraju, *Accounts of Chemical Research*, 2002, **35**, 565-573.
78. M. Saggu, N. M. Levinson and S. G. Boxer, *Journal of the American Chemical Society*, 2012, **134**, 18986-18997.
79. M. E. Bluhm, M. Ciesielski, H. Görls and M. Döring, *Angewandte Chemie International Edition*, 2002, **41**, 2962-2965.
80. L. Cai-Ming, G. Hong-Yun, Z. De-Qing and Z. Dao-Ben, *Letters in Organic Chemistry*, 2005, **2**, 712-717.

ha formattato: Italiano (Italia)

ha formattato: Italiano (Italia)

ha formattato: Italiano (Italia)

CRediT author statement

Emanuele Priola: Conceptualization, Data curation, Methodology, Investigation, Writing- Original draft preparation. **Eleonora Conterosito**: Conceptualization, Data curation, Methodology Writing- Original draft preparation. **Alessia Giordana**: Visualization, Investigation and Conceptualization. **Giorgio Volpi***:* Supervision, Validation. **Claudio Garino**: Supervision, Validation, **Luca Andreo:** Software and Validation, **Eliano Diana:** Writing- Reviewing and Editing, **Claudia Barolo:** Writing- Reviewing and Editing, **Marco Milanesio:** Writing- Reviewing and Editing,